On the Thermoelastic Influence of Fluid-Gas Phase Transition Pressure on the Closed Structural Storage Container

JACOB NAGLER
NIRC,
Haifa, Givat Downes
ISRAEL

Abstract: - The current paper presents a finite element method (FEM) axisymmetric solution based on commercial software for an isotropic closed-ended container filled with fluid, located in the triple point phase (liquefied gas) while being converted into gas through a phase transition to critical point phase by a simultaneously rapid change of pressure and temperature to their critical values. The whole chemical process will be simulated through thermo-elastic analysis that is controlled by temperature-displacement dynamic coupling and subjected to step function boundary conditions alongside liquefied triple point initial conditions. In the process, the maximum principal stresses will be determined and illustrated as dependent on the container thickness. In the process, investigation will be carried out for prominent parameters, like, container hollow geometry type (spherical, ellipsoidal, and cylindrical) and raw material of the container. Commercial software solution calibration against existing literature solutions has been performed. Also, the solution accuracy was examined by element size mesh analysis to be coherent. In conclusion, the best materials to use were Molybdenum TZM and Tungsten while the preferred shape is the ellipsoidal shape. However, a typical vessel that is still durable with sufficient thermal strength for gas storage purposes is a cylinder body container with spherical ended cups made from Aluminum 6061 T6.

Key-Words: FEM, thermal shock, thermo-elasticity, storage container, phase transition.

Received: October 28, 2022. Revised: August 16, 2023. Accepted: September 27, 2023. Published: October 11, 2023.

1 Introduction

A closed geometry of container or tank with ended caps filled with liquefied gas that can turn into gas by conversion based on evaporation is an important mechanism in the chemical industry, [1], [2], [3], [4], [5]. Those tanks have to withstand both thermal and mechanical pressure loads that act on them in various configurations (internal, external, simultaneously, or alternating).

A guide for tanks design was produced by, [1], in 1982. These containers might be used for testing or containing different propellants or different Cryogenic materials, [2]. They also might be used for chemical processes understanding of boiling and condensation, [3]. In the aerospace industry they might be used as pilot oxygen suppliers or fuel tanks, [4]. They could be made from homogenous material or composite, [4]. A thorough review concentrating on the applications of the liquid-vapor phase has just shed light recently, [5].

The current paper concentrate on the controllability of shape-changing container under constant volume, varying from cylinder to spherical geometry through elliptic/spheroidal shape subjected to thermo-mechanical shock/impact loading. The parameters of influence that will be examined during the thermo-elastic impact analysis are: (1) different gas types (Oxygen, Hydrogen, and Nitrogen) (2) Container material (Al 6061 T6, Cres 304, Molybdenum TZM, Titanium, and Tungsten). In the future, the effect of external convection should be examined.

Many studies have been performed over the decades on the thermo-elastic impact coupling over an ended cap tank containing liquefied gas. Starting with, [6], who investigated analytically the bursting pressure of cylindrical and spherical vessels. The study, [7], modeled multilayered composite hydrogen storage tanks by FEM ANSYS code. Six years later, [8], have developed FEM Analysis for FGM composite material (graphite epoxy) containing hydrogen and including phase transition based on ANSYS code. The study, [9], dealt with Carbon dioxide critical shock by reaching from the triple point to the critical point based on pressure and temperature coupling raising. The study, [10], has developed a linear thermo-elastic solution for the cases of decanting and refilling tank processes.

The current essay problem is characterized by a refilling tank process that combines critical shock that is generated due to both pressure and temperature uprising from the triple point to the critical point. As a result, due to internal processes, a large amount of energy within a limited space might rapidly be released to create the explosion. Some recent progress on the critical point importance in the context of shock waves and safety precautions using CFD analysis was performed by, [11].

FGM and composite vessels were also have been a focus of the investigation. For instance, [12], conducted a study with FGM thermo-elastic modeling time-dependent but no impulse or shock wave were exhibited. The study, [13], examined the multilayered composite pressure vessel considering the influence of the closed ends and thermo-elastic phenomenon under steady-state conditions. Wave propagation into the environment after burst, shock, or impulse is well documented by, [14], while the severe influence on crack propagation behavior is well reported by, [15].

The current study provides stresses and displacement results through investigation of isotropic hollow closed-ended container or tank vessel under internal short pulses of pressure and temperature loading (~1 micro-meters) based on finite element method (FEM) commercial software (Abaqus). The modeling and pulse duration will be based on former studies in the field, done by, [16], who are concerned with spherical pressure vessels subjected to both temperature and pressure loading. The criteria for crack initiation include principal stress (tension mechanism) and Cowper-Symonds comparative criterion (shear and tension mixed mechanism), [17]. In addition, based on the proposed modeling suggested by, [18], studies by, [19], [20], [21], (thorough investigation of FGM cylindrical and spherical shell without ended cups under internal pressure and thermal pulse loading) and triple point modeling by, [22].

Pulse (duration) estimation appears in the classical, [23], study (estimate pulse duration dependent on material thickness to wave velocity ratio) and by recent papers, [24], (deal with the detonation pulse of time duration), [25], (give some sense of time on pulse duration dependent on material). While for long time periods with similarly discussed modeling of thermal shock on closed-ended vessel cylinders see, [26]. Note that the case of reactive pressure vessels (RPV) and pressurized thermal shock (PTS) in the context of nuclear reactions are well documented by, [27], a similar model as presented in the current text.

The whole chemical process inside the container will be simulated here through thermo-elastic impulse analysis that is controlled by temperature-displacement dynamic coupling and subjected to step function boundary conditions alongside liquefied triple point initial conditions. In the process, the maximum principal stresses will be determined and illustrated as dependent on the container thickness. In the process, investigation will be carried out for prominent parameters, like, container hollow geometry type (spherical, ellipsoidal, and cylindrical) and raw material of the container.

2 FEM – Geometrical Examination

To efficiently investigate those mentioned models the input data that includes geometrical and material properties (M.P.) alongside boundary conditions (B.C.) and initial conditions (I.C.) will be introduced by separate tables that fit the analysis configuration steps and parameters examined.

The following equations to calculate Lame' constants (λ, μ) and wave velocity (V) are:

$$\lambda = \nu E/(1+\nu)(1-\nu) \quad (1)$$

$$\mu = E/2(1+\nu) \quad (2)$$

$$V_e = \sqrt{E(1-\nu)/\rho(1+\nu)(1-2\nu)} = \sqrt{(\lambda+2\mu)/\rho} \approx \sqrt{(\frac{Bulk_{Modulus}}{\rho})} \quad (3)$$

where E, ν, ρ represent Young's modulus, Poisson's ratio and density, respectively. It is also known that the steady-state axial ($\sigma_{a\_cylinder}$), circumference/tangential ($\sigma_{\theta\_cylinder}$) and radial ($\sigma_{r\_cylinder}$) stresses developed in thick shell cylinder are, [29]:

$$\sigma_{a\_cylinder\_thick} = \frac{p_i r_i^2 - p_o r_o^2}{r_o^2 - r_i^2} \quad (4)$$

$$\sigma_{\theta\_cylinder\_thick} = \frac{p_i r_i^2 - p_o r_o^2}{r_o^2 - r_i^2} - \frac{r_i^2 r_o^2 (p_o - p_i)}{r^2 (r_o^2 - r_i^2)} \quad (5)$$

$$\sigma_{r\_cylinder\_thick} = \frac{p_i r_i^2 - p_o r_o^2}{r_o^2 - r_i^2} + \frac{r_i^2 r_o^2 (p_o - p_i)}{r^2 (r_o^2 - r_i^2)} \quad (6)$$

It is also known that the steady-state circumference/tangential (σ_{θ_sphere}) and radial (σ_{r_sphere}) stresses developed in thick shell spheres are [29]:

$$\sigma_{r\_sphere\_thick} = p_o \frac{r_o^3}{r^3} \frac{r^3 - r_i^3}{r_i^3 - r_o^3} + p_i \frac{r_i^3}{r^3} \frac{r_o^3 - r^3}{r_i^3 - r_o^3} \quad (7)$$

$$\sigma_{\theta\_sphere\_thick} = p_o \frac{r_o^3}{2r^3}\frac{2r^3+r_i^3}{r_i^3-r_o^3} + p_i \frac{r_i^3}{2r^3}\frac{r_o^3+2r^3}{r_i^3-r_o^3} \quad (8)$$

In the case of thin shell cylinders, the well-known formulations are:

$$\sigma_{a_{cylinder_{thin}}} = \frac{p_i 2r_i}{4t} \quad (9)$$

$$\sigma_{\theta_{cylinder_{thin}}}(Max.Principal) = \frac{p_i 2r_i}{2t} \quad (10)$$

$$\sigma_{r_{cylinder_{thin}}} \approx 0 \quad (11)$$

In the case of thin shell spheres, the well-known formulations are:

$$\sigma_{a_{sphere_{thin}}} = \frac{p_i 2r_i}{4t} \quad (12)$$

$$\sigma_{\theta_{sphere_{thin}}}(Max.Principal) = \sigma_{a_{sphere_{thin}}} \quad (13)$$

$$\sigma_{r_{sphere_{thin}}} \approx 0 \quad (14)$$

where p_i, p_o, r_i, r_o, t represent the internal pressure, outer pressure, internal radius, outer radius, and thickness, respectively.

A. Data Modelling

In this stage five hollow kinds of geometrical cup-ended tanks will be examined: (i) Spherical (r – denote the sphere radius), (ii) Elliptical (a, b, c denote the ellipse radii), and (iii) Cylindrical (H, r denote the cylinder height and radius, respectively, while three types of ended cups cylinder tank are examined) as appear in Figure 1 (Appendix). All five shapes share the same volume constant value ($20\,[liter]$) and thickness (10 mm). Also, all five tank shapes are made of isotropic material with the same initial and boundary conditions as indicated and summarized in Table 1 (Appendix). Each container contains oxygen-liquefied gas that is converted through evaporation into gas, moving from triple point to critical point phase diagram (pressure and temperature increase) by pulse duration rate of $20\mu sec$ as appear in Figure 2 (Appendix) and Table 2 (Appendix). The chosen gas for all cases in this section will be Oxygen because of its high pressure and thermal differences it creates great thermo-mechanical shock over a small pulse duration compared to the alternative gases appeared in Table 2 (Appendix). However, a hidden assumption is that both temperature and pressure increase at the same rate of time. In addition, we assume that the whole liquid is heated and pressurized homogenously, while transformed to mechanical pressure and thermal loading that act directly on the container walls through a shock wave mechanism using ramp function $H(t)$. The FEM representation of all five configurations (number of elements, element size, and type) appears in Figure 3 (Appendix) alongside mesh properties in Table 3 (Appendix).

B. FEM analysis results in comparison and discussion of thermo-elastic shock behavior for all geometrical cases

The FEM solution is associated with explicit dynamic temperature-displacement analysis using axisymmetrical conditions (elements, model, etc.) in cylindrical coordinates. The discussion will be limited to the container crucial regions which will be divided into two regions: (i) the internal wall edge in the middle of the cylinder length and (ii) the cup regions – while both areas initially absorb most of the heat and stress developed as a result of direct activation of coupled thermal and pressure loadings. Maximum principal stresses together with radial and longitudinal displacement profile values of each configuration will be presented in an appropriate figure.

To examine the results' magnitude value, even though the analysis concentrates on the – structural dynamic (impulse) problem, yet, the steady–state classical formulation (4) – (8) might give the reader some sense about the stress order of magnitude. In Table 4 (Appendix), two examined geometrical configurations stress results are exhibited.

Analysis of Figure 4 (Appendix) (*a*)-(*c*) regarding the container body shapes raises the following comprehensions:

- Observing Figure 2 (*a*-*b*) (Appendix) might lead to understanding that the spherical shape body of the container has the largest radial and longitudinal profile displacement value relative to the ellipsoidal, cylinder with spherical end cups (CSE), straight-ended cylinder configuration (CSTE) and mixed straight and spherical ended (CME) configuration.
- The smallest radial displacement profile value is attached to the ellipsoidal shape.
- All displacement radial profile values were found to be in the same order (~ few hundredsμm) and share similar qualitative behavior.
- All longitudinal displacement profile values were found to be in the same order while approaching zero as derived from Figure 4*b* (Appendix).
- Note that the maximum displacement profile values for all examined container body section cases were considered at the internal edge location in the middle of the container body length.
- The obtained maximum principal stresses for all container-body cases appeared in Figure 4*c* (Appendix) were found to have the same order of

magnitude which is consistent with the mentioned radial displacements sharing the same order of magnitude in Figure 4a (Appendix).

- Moreover, the measured wave amplitude per time point is decreased relative to adjacent time point in cases where the surface increases according to $2\pi r \cdot h$ in cylinder case, $2\pi r \cdot 2r$ in sphere case and $2\pi a^2 \sqrt{1+\frac{c^2}{a^2-c^2} arctanh\left(\frac{a^2-c^2}{a^2}\right)}$ in the spheroid case, unlike wave propagating in a rectangular bar section that keeps unvaried amplitude due to its constant section.
- The cylinder and sphere maximum principal stress values obtained by analysis are in the same order of magnitude as classical shell theory (Table 4 (Appendix) vs. Figure 4*c* (Appendix)) but their numerical value is two times higher than the literature theory due to the dynamic impulse and thermal loading considered during the analysis process.

Analysis of Figure 5 (*a*)-(*d*) (Appendix) regarding the container cup shapes region raises the following comprehensions:

- Observing Figure 5*a* (Appendix) at the end cups region of the spherical, ellipsoid, and cylindrical containers (CSE, CSTE, and CME) shows that all radial displacement results from profile values approach zero value.
- However, CSTE and CME cups share identical longitudinal displacement profile values in their straight cup regions (~10e-3), while having relatively meaningful magnitude over the other profiles (~10e-6), as exhibited in Figure 5(*b*)-(*c*) (Appendix). Although one might observe that the time required to complete the full displacement wavelength is larger than 2e-4 [sec].
- The obtained maximum principal stress profile values presented in Figure 5(*d*) (Appendix) seem to have similar wavy qualitative behavior except for the spherical cup container that shows significant large values (~1GPa) over all other kinds of cylinder platforms cup shapes which share similar behavior profiles (~100 - 400 MPa).

- **In conclusion**,

○ Also, the ellipsoidal shape (body and cups) container was found to have the least stress and displacement profile values.

○ The spherical body container was found to have the maximum principal stresses and displacement profile values.

The region of the cup unlike the container body – part experienced high temperatures and stresses due to its limited geometrical region that passes the stress and heat fluxes through curved radius geometry, as so, absorbs a large amount of energy that causes an accumulation of stresses due to the transition bending radius.

3 FEM – Materials Examination

A. Data Modelling

In this section different types of materials will be examined for the case of cylinders with spherical ends which is very common for storage use in many industries and has relatively good resistance to heat and pressure as proved earlier in the previous Sec. 2. The geometrical properties as well as B.C, I.C., gas (Oxygen) and mesh are the same as appear in Table 1 (Appendix), Table 2 (Appendix) and Table 3 (Appendix).

The only variable parameter is the container material which will be examined in this section and elaborated in Table 5 (Appendix). The chosen materials that will be examined to cope with the high fluxes and stresses are Al 6061 T6, Cres 304, Molybdenum TZM, Titanium, and Tungsten.

B. FEM analysis results comparison and discussion of thermo-elastic shock behavior for all material cases

Based on the previous investigation, the examined results for comparison between different materials' durability will be the radial stress, the longitudinal stress, and the shear stress accompanied by the appropriate displacements through a dynamic temperature-displacement axisymmetric analysis with a total analysis time of $2 \cdot 10^{-4}$ [sec].

Analysis of Figure 6 (*a*)-(*b*) (Appendix) regarding the container body and cup shapes regions made of different materials raises the following comprehensions:

- Observing Figure 6(*a*) - (*b*) (Appendix) teaches that Molybdenum TZM and Tungsten are very strength-efficient materials to use to decrease the developed maximum principal stresses in the whole container regions. Also, they share the same profile and magnitude of order values.
- The less strength-efficient materials in the whole container regions which also share the same profile and magnitude of order are profiles Cres 304 and Titanium.
- However, the Al 6061 T6 profile qualitatively behaves as Cres 304 and Titanium, except that its numerical values range is laid between

Molybdenum TZM & Tungsten and Cres 304 & Titanium, which makes it a cheap and reliable strength material to use and apply.

4 Conclusion

Investigating five types of pressure vessels by Abaqus commercial software in the aspects of shape and material in the context of thermoelastic impulse has led to the conclusion that the best materials to use are Molybdenum TZM and Tungsten while the preferred shape is the ellipsoidal shape. However, from manufacturing and economic aspects, a typical type that is durable enough with sufficient strength against thermo-mechanical impact loadings for gas storage purposes is a cylinder body container with spherical ended cups made from Aluminum 6061 T6.

References:

[1] Fecht, B. A., Gates, T. E., Nelson, K. O., Marr, G. D., (1982) *Comparative safety analysis of LNG storage tanks*, Report, U.S. Department of Energy, DE-AC06-76RLO 1830. https://www.osti.gov/servlets/purl/6635203 (Accessed Date: 07/06/2023)

[2] Bellur, K *et al*. (2016) A new experiment for investigating evaporation and condensation of cryogenic propellants, *Cryogenics* 74, pp.131-137. DOI: 10.1016/j.cryogenics.2015.10.016

[3] Kharangate, C. R., Mudawar, I., (2017) Review of computational studies on boiling and condensation, *IJHMT*, 108, 1164-1196. DOI:10.1016/j.ijheatmasstransfer.2016.12.065

[4] Tapeinos, I. (2019). *Multi-Spherical Composite-Overwrapped Cryogenic Fuel Tanks for Hypersonic Aircrafts*, MSC Thesis, Delft University. DOI: 10.4233/uuid:850a6ccc-7686-4536-8469-418691dc2dbb

[5] Zuo, Z., Zhu, W., Huang, Y., Wang, L., Tong, L., (2023) A review of cryogenic quasi-steady liquid-vapor phase change: Theories, models, and state-of-the-art applications, *IJHMT*, 205, 123916. DOI:10.1016/j.ijheatmasstransfer.2023.123916

[6] Cumalioglu, I., (2005) Modeling and simulation of a high-pressure hydrogen storage tank with dynamic wall, *Engineering*. DOI: http://hdl.handle.net/2346/1035 (Accessed Date: 07/06/2023)

[7] Svensson, N. L. (1958) The bursting pressure of cylindrical and spherical vessels, *ASME. J. Appl. Mech.* 25, pp.89-96. DOI: 10.1115/1.4011694

[8] Badri T. M., and Al-Kayiem, H. H., (2011) Numerical analysis of thermal and elastic stresses in thick pressure vessels for cryogenic hydrogen storage apparatus. *Journal of Applied Sciences*, 11, pp.1756-1762. DOI: 10.3923/jas.2011.1756.1762

[9] van der Voort, M.M., van den Berg, A.C., Roekaerts, D.J.E.M., Xie, M., de Bruijn, P.C.J., (2012) Blast from explosive evaporation of carbon dioxide: experiment, modeling and physics. *Shock Waves*, 22, pp.129–140. DOI: 10.1007/s00193-012-0356-0

[10] Liu, Z,, *Temperature and Stress Analysis during Tank Decanting and Refilling Process* (2018). Thesis, Lincoln, Nebraska. https://digitalcommons.unl.edu/engmechdiss/44 (Accessed Date: 07/06/2023)

[11] Ustolin, F., Tolias, I. C., Giannissi, S. G., Venetsanos, A. G., Paltrinieri, N., (2022) A CFD analysis of liquefied gas vessel explosions Process, *Saf. Environ. Protect*., 159, pp.61-75. DOI: 10.1016/j.psep.2021.12.048

[12] Vaziri, S. A., Ghannad, M., Bég, O. A., (2019) Exact thermoelastic analysis of a thick cylindrical functionally graded material shell under unsteady heating using first order shear deformation theory, *Heat Transfer—Asian Res*., 48, pp.1737- 1760. DOI: 10.1002/htj.21455

[13] Zhang, Q., Wang, Z. W., Tang, C. Y., Hu, D. P., Liu, P. Q., Xia, L. Z., (2012) Analytical solution of the thermo-mechanical stresses in a multilayered composite pressure vessel considering the influence of the closed ends, *IJPVP*, 98, pp.102-110. DOI: 10.1016/j.ijpvp.2012.07.009

[14] Oliver, S., Simpson, C., Collins, D. M., Reinhard, C., Pavier, M., Mostafavi, M., (2021) In-situ measurements of stress during thermal shock in clad pressure vessel steel using synchrotron X-ray diffraction, 192, 106136. DOI: 10.1016/j.ijmecsci.2020.106136

[15] Xiao, J., Breitung, W., Kuznetsov, M., Zhang, H., Travis, J. R., Redlinger, R., and Jordan, T., (2017) GASFLOW-MPI: A new

3-D parallel all-speed CFD code for turbulent dispersion and combustion simulations Part II: First analysis of the hydrogen explosion in Fukushima Daiichi Unit 1, 42, *IJHE*, pp.8369-8381. DOI: 10.1016/j.ijhydene.2017.01.219

[16] Wang, Q., Sun, Y., Li, X., Shu, C. M., Wang, Z., Jiang, J., Zhang, M., and Cheng, F., (2020) Process of natural gas explosion in linked vessels with three structures obtained using numerical simulation, *Processes* 8, 52. DOI: 10.3390/pr8010052

[17] Lu, S., Wang, W., Chen, W., Ma, J., Shi, Y., Xu, C., (2019) Behaviors of thin-walled cylindrical shell storage tank under blast impacts, *Shock and Vibration*, 6515462, pp.1-21. DOI: 10.1155/2019/6515462

[18] Ramamurthi, K., (2021) *Modeling explosions and blast wave*, Springer India 2nd edn, pp.257-271. DOI:10.1007/978-3-030-74338-3_3

[19] Chao, T.W., and Shepherd, J. E., (2005) Fracture response of externally flawed aluminum cylindrical shells under internal gaseous detonation loading. *Int J Fract*, 134, pp.59-90. DOI: 10.1007/s10704-005-5462-x

[20] Shepherd, J. E., (2007) *Structural Response to Explosions*, 1st European Summer School on Hydrogen Safety University of Ulster.

[21] Verma, K. P., Maiti, D. K., (2021) Transient analysis of thermo-mechanically shock loaded four-parameter power law functionally graded shells, *Composite Structures* 257, 113388. DOI: 10.1016/j.compstruct.2020.113388

[22] H. Z. Xi, D. R. Kong, Y. Q. Peng, Q. Shi, S. M. Zhang & G. G. Le (2022) The triple point path prediction model based on geometric method, Journal of Energetic Materials, DOI: 10.1080/07370652.2022.2140859

[23] Frederick, C. J., Kassoy D. R. and Riley, N., (1984) Shocks generated in a confined gas due to rapid heat addition at the boundary. I. Weak shock waves *Proc. R. Soc. Lond. A* 393309-329. DOI: 10.1098/rspa.1984.00

[24] Frolov, S. M., Shamshin, I. O. and Aksenov, V. S. (2022) Deflagration-to-detonation Transition in Stratified Oxygen – Liquid Fuel Film Systems, Combustion Science and Technology, 194:16, pp.3432-3466, DOI: 10.1080/00102202.2021.1929196

[25] Wang, A., Yu, X., Wang, H., Li, Y., Zhang, J., Fan, X., (2022) Dynamic response of Sandwich tubes with continuously density-graded aluminum foam cores under internal explosion load. Materials (Basel)., 15, 6966. DOI: 10.3390/ma15196966.

[26] Murugan, S., Starvin, M.S., Dhas, K. M., (2013) Thermo structural analysis of high-pressure cryogenic tank, *IJERT*, 2 1730-1738. https://www.ijert.org/research/thermo-structural-analysis-of-high-pressure-cryogenic-tank-IJERTV2IS110549.pdf (Accessed Date: 07/06/2023)

[27] Chen, W., Dai, S.m and Zheng, B., (2022) Continuum damage dynamic model combined with transient elastic equation and heat conduction equation to solve RPV stress, *Fractal and Fractional* 6, 215. DOI: 10.3390/fractalfract6040215

[28] Source for material properties: https://www.matweb.com/ (Accessed Date: 07/06/2023)

[29] Krivoshapko, S. N. (2007) Research on general and axisymmetric ellipsoidal shells used as domes, pressure vessels, and tanks. *ASME. Appl. Mech. Rev*. 60, pp.336–355. DOI: 10.1115/1.2806278

APPENDIX

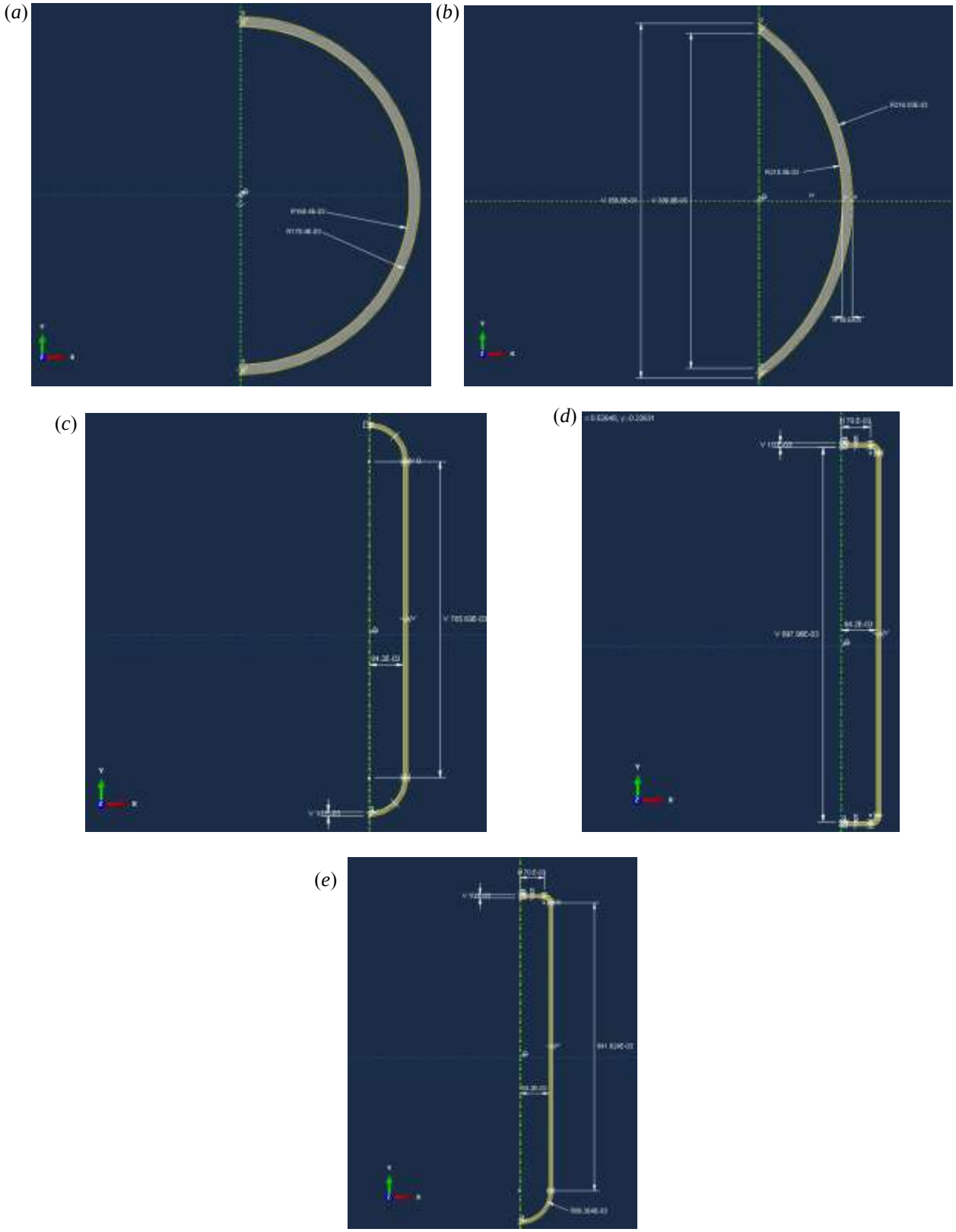

Fig. 1: Axi-symmetric geometric section configurations: (*a*) Spherical (*b*) Elliptical (*c*) Cylindrical with spherical ends (*d*) Cylindrical with straight ends (*e*) Cylindrical with mixed ends.

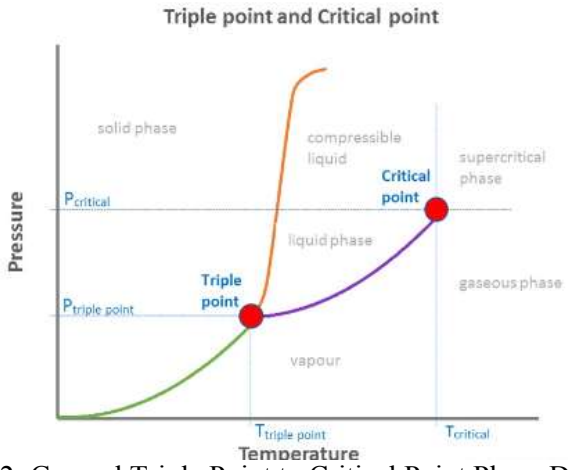

Fig. 2: General Triple Point to Critical Point Phase Diagram.

(*a*)

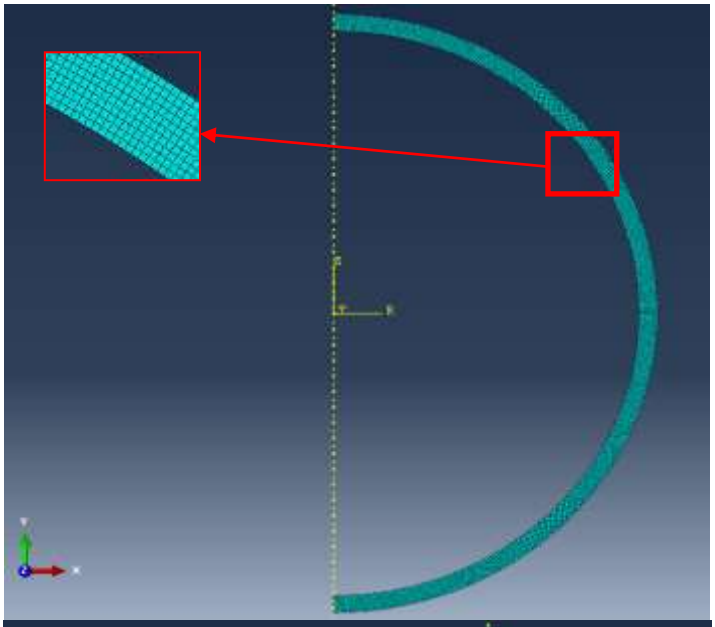

(*b*)

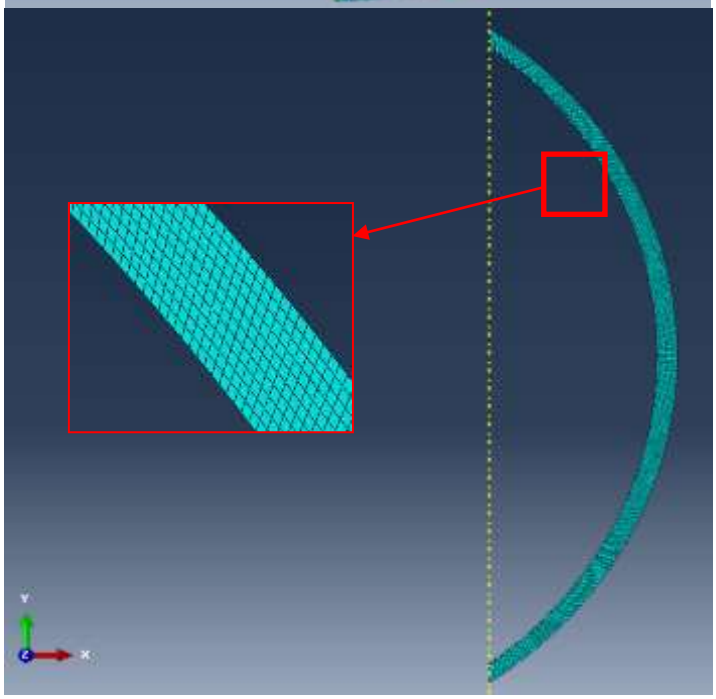

(*c*)

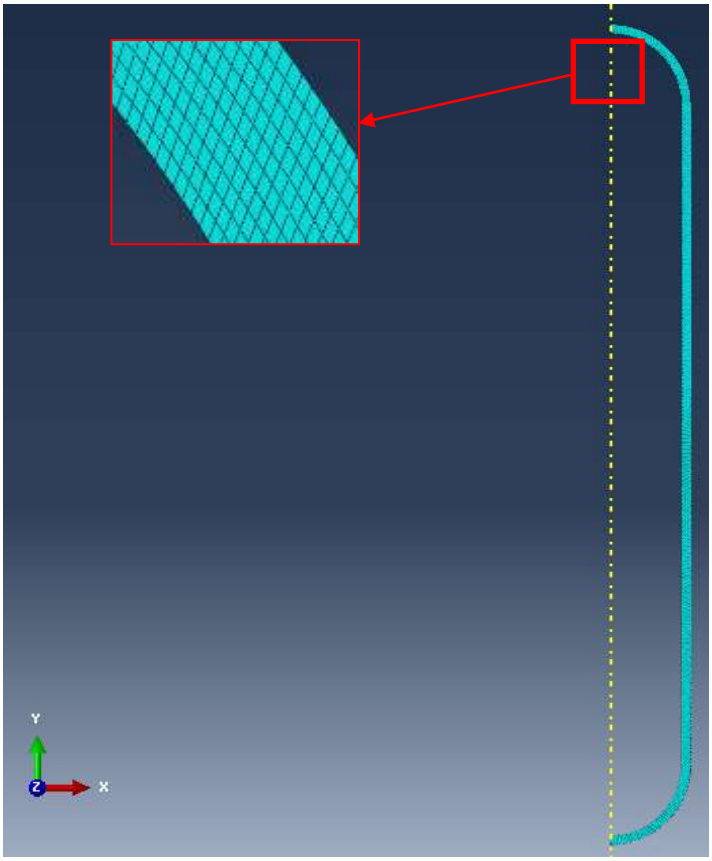

(*d*)

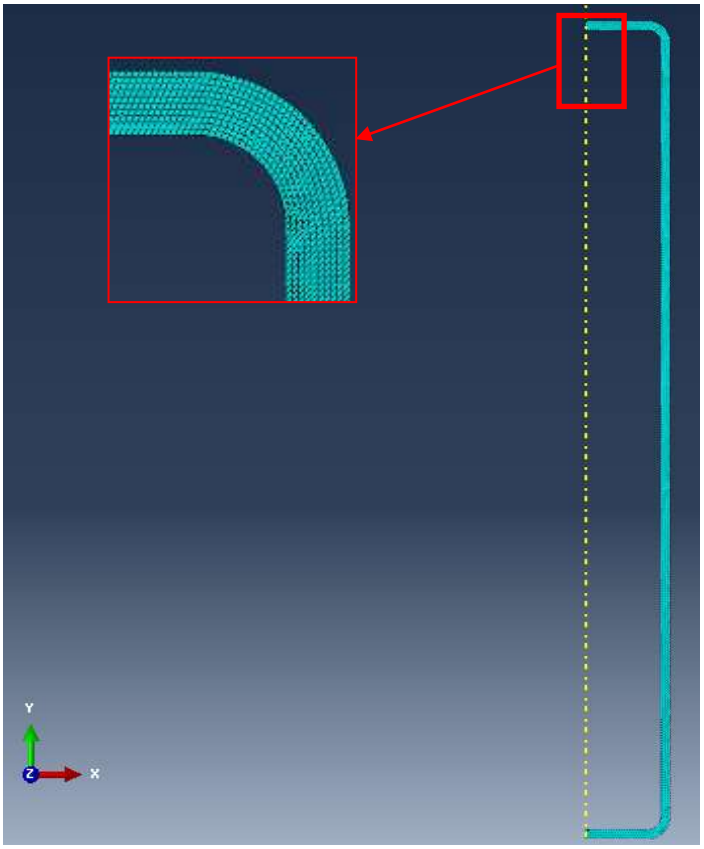

(*e*)

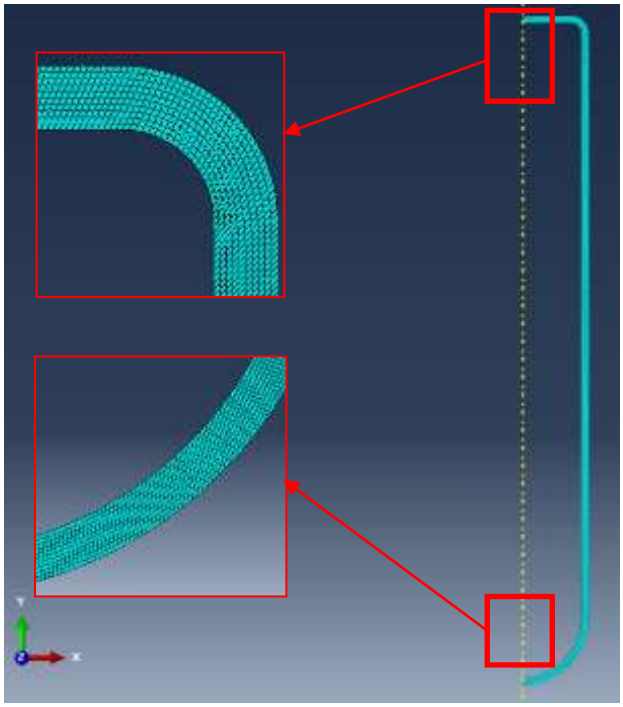

Fig. 3: Axi-symmetric FE model's configurations: (*a*) Spherical (*b*) Elliptical (*c*) Cylindrical with spherical ends (*d*) Cylindrical with straight ends (*e*) Cylindrical with mixed ends.

Table 1. Container geometrical properties per B.C., I.C. & M.P. cases for three types of container shapes as input data for the FEM

Physical Property	Value [M.K.S.]	Formula
Geometrical features	Fig. 1	$V\,(spherical) = \frac{4}{3}\pi r^3$ $V\,(cylindrical) = \pi r^2 H_1$ $V\,(ellipsoid) = \frac{4}{3}\pi abc$
Mechanical Loading Case	$P(r_i,t) = H(t)$	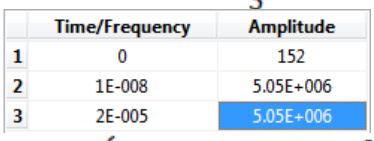 $H(t) = \begin{cases} t \le 0: P_{Triple-Point}[Pa] \\ t > 0: P_{Critical-Point}[Pa] \end{cases}$
Mechanical Boundary Conditions Case	$u_{i,t\le 0} = Free$ $u_{t>0} = Free$	--
Thermal Boundary Conditions Case	$T(r,t) = H(t)$ $T_{i,t\le 0} = T_{Triple-Point}{}^0C$	$H(t) = \begin{cases} t \le 0: T_{Triple-Point}[\,^0C] \\ t > 0: T_{Critical-Point}[\,^0C] \end{cases}$ 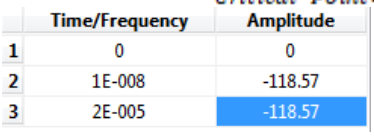
Material Properties	Cres 304 from MATWEB, [28]	
Density (ρ) [kg/m^3]	8000	--
Poisson' ratio (ν)	0.29	--
Young Modulus of Elasticity (E) [GPa]	193	--
Thermal Conductivity]W/m ^0C[	16.2	--
Thermal Expansion Coefficient $[1/\,^0C]$	$4.05 \cdot 10^{-6}$	--
Specific Heat Capacity, C_p [J/kg ^0C]	500	--
Wave velocity (V_e) [m/sec]	5131	--
Lame' Constant $\lambda\,[GPa]$	61	--
Lame' Constant $\mu\,[GPa]$	74.81	--
Characterization Time of Wave [sec]	$1.95 \cdot 10^{-6}$	$\frac{thickness}{V_e}$
Total Analysis time [sec]	$2 \cdot 10^{-4}$	

Table 2 Gas triple and critical points data

Gas type	Temperature – T. P. [^{0}C]	Pressure – T.P. [kPa]	Temperature – C. P. [^{0}C]	Pressure – C.P. [Bar]
Hydrogen	-259.31	7.04	-240	13.0
Oxygen	-218.79	0.152	-118.6	50.5
Nitrogen	-209.97	12.6	-147	34.0

Table 3. Abaqus software FEM analysis data

Element mesh rules details (No., size, type)
Type: Axi-symmetric, CAX4RT, quad.
Number of elements per configuration is in the range: of 4050 - 10830.
Size: 1 [mm]
Analysis type: plain – strain.
Dt=1e-7 sec.

Table 4. Geometrical configuration (Body part) versus developed stress through classical shell theory analysis

Configuration/Stress At $r = r_i$	Geometrical and Pressure Data	Radial Stress [Bar]	Axial Stress [Bar]	Tangential Stress [Bar]
Sphere	$p_o = 0$ $p_i = 50.5\,[bar]$ $r_i = 170\,[mm]$ $r_0 = 180\,[mm]$	50.5	430.2	430.2
Cylinder	$p_o = 0$ $p_i = 50.5\,[bar]$ $r_i = 84.2\,[mm]$ $r_0 = 94.2\,[mm]$	50.5	200.7	451.9

Table 5. Types of container material properties from MATWEB, [28]

Material Properties	Al 6061 T6	Cres 304	Molybdenum TZM	Titanium	Tungsten
Density (ρ) [kg/m^3]	2700	8000	10160	4500	19300
Poisson' ratio (ν)	0.33	0.29	0.29	0.34	0.28
Young Modulus of Elasticity (E) [GPa]	68.9	193	325	116	400
Thermal Conductivity]W/m ^0C[	167	16.2	118	17	150
Thermal Expansion Coefficient $[1/\,^0C]$	$6.90 \cdot 10^{-5}$	$4.05 \cdot 10^{-6}$	$4.65 \cdot 10^{-5}$	$7.155 \cdot 10^{-6}$	$5.8 \cdot 10^{-5}$
Specific Heat Capacity, [J/kg ^0C] C_p	896	500	250	528	134
Wave velocity (V_e) [m/sec]	6149	5131	6475	6300	5147
Characterization of Time Wave [sec]	$1.63 \cdot 10^{-6}$	$1.95 \cdot 10^{-6}$	$1.55 \cdot 10^{-6}$	$1.59 \cdot 10^{-6}$	$1.94 \cdot 10^{-6}$

(*a*)

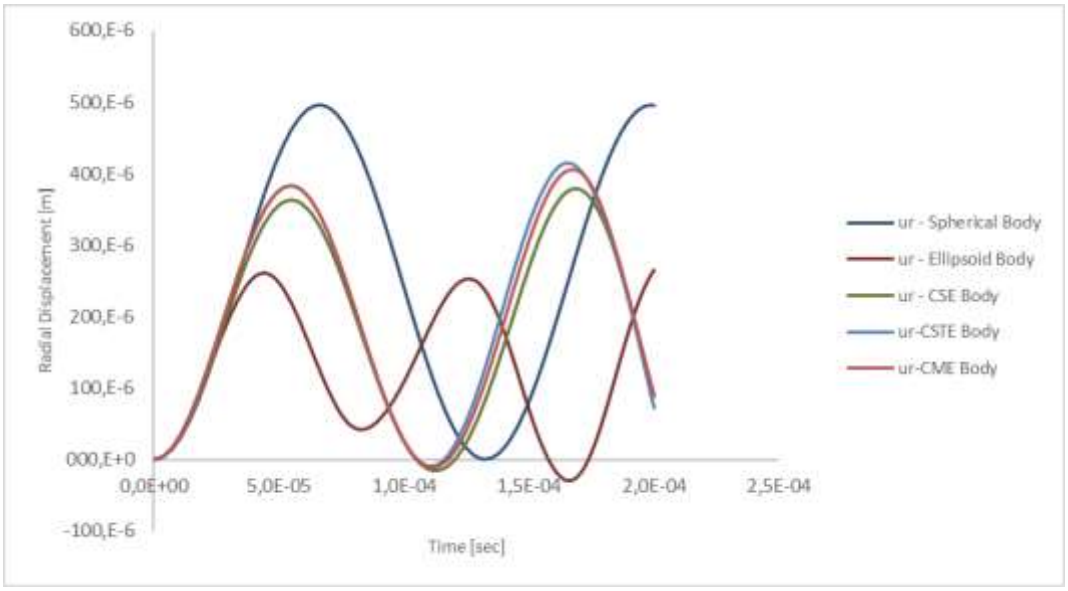

(*b*)

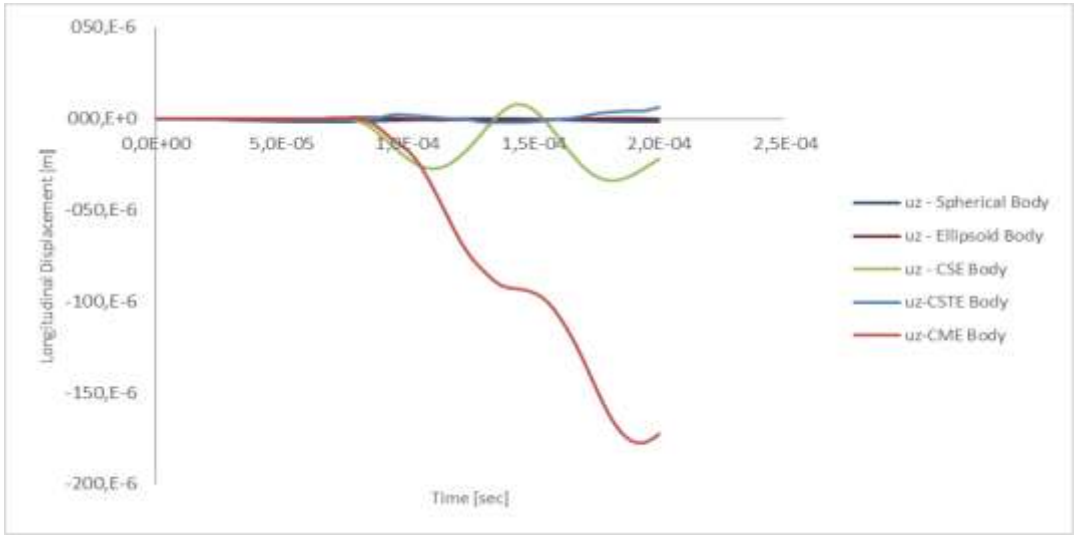

(*c*)

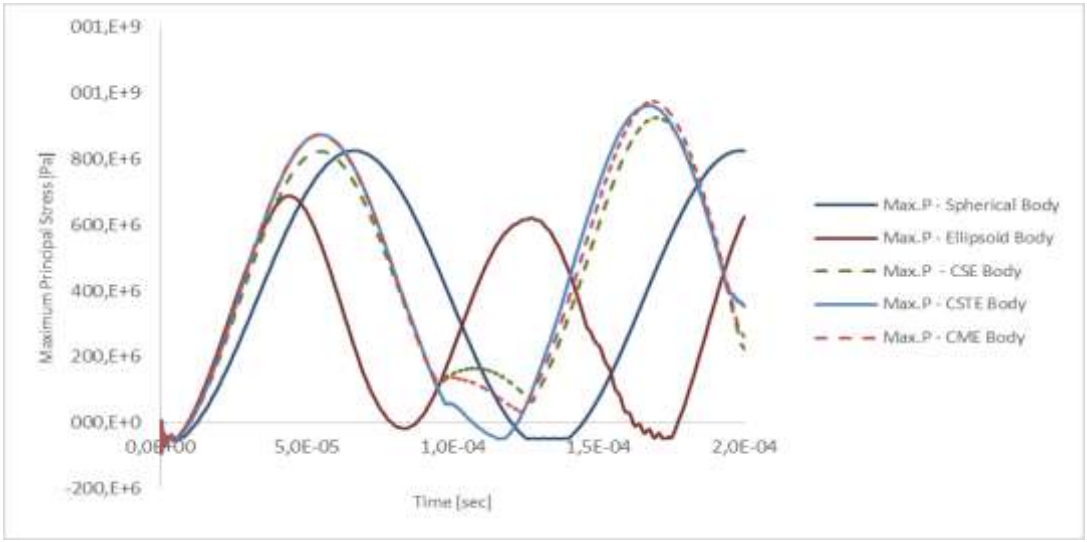

Fig. 4: FE model results for several container body-part shapes: (*a*) u_r - radial displacement for spherical, ellipsoid, CSE, CSTE, and CME (*b*) u_z – the longitudinal displacement for spherical, ellipsoid, CSE, CSTE, and CME shapes (*c*) Maximum principal stress for spherical, ellipsoid, CSE, CSTE, and CME shapes.

(*a*)

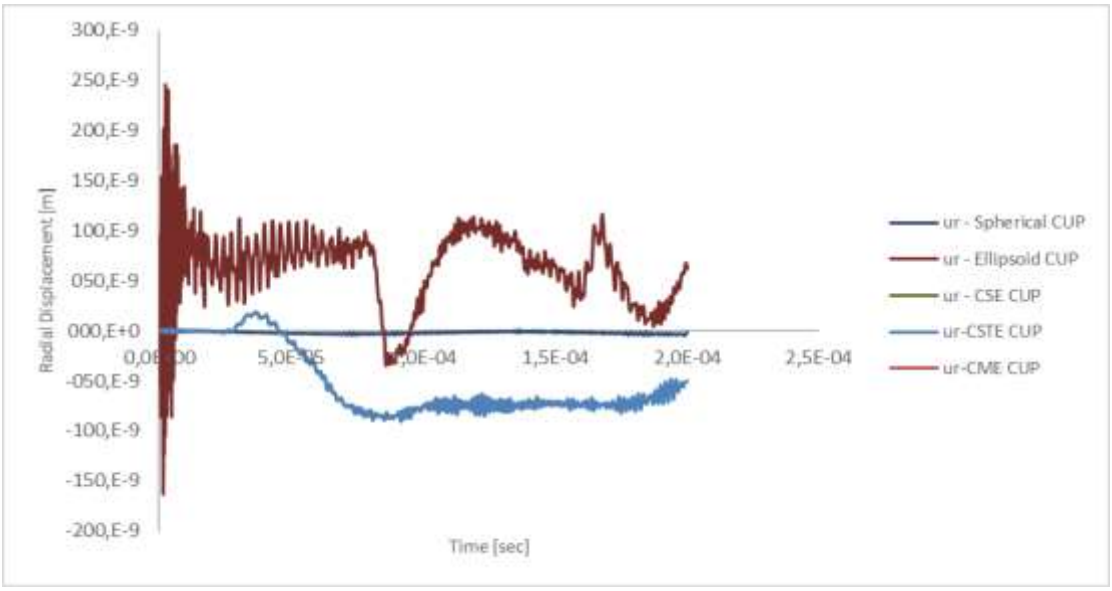
300,E-9
250,E-9
200,E-9
150,E-9
100,E-9
050,E-9
000,E+0
-050,E-9
-100,E-9
-150,E-9
-200,E-9
Radial Displacement [m]
5,0E-05
1,5E-04
2,0E-04
2,5E-04
Time [sec]
ur - Spherical CUP
ur - Ellipsoid CUP
ur - CSE CUP
ur-CSTE CUP
ur-CME CUP

(*b*)

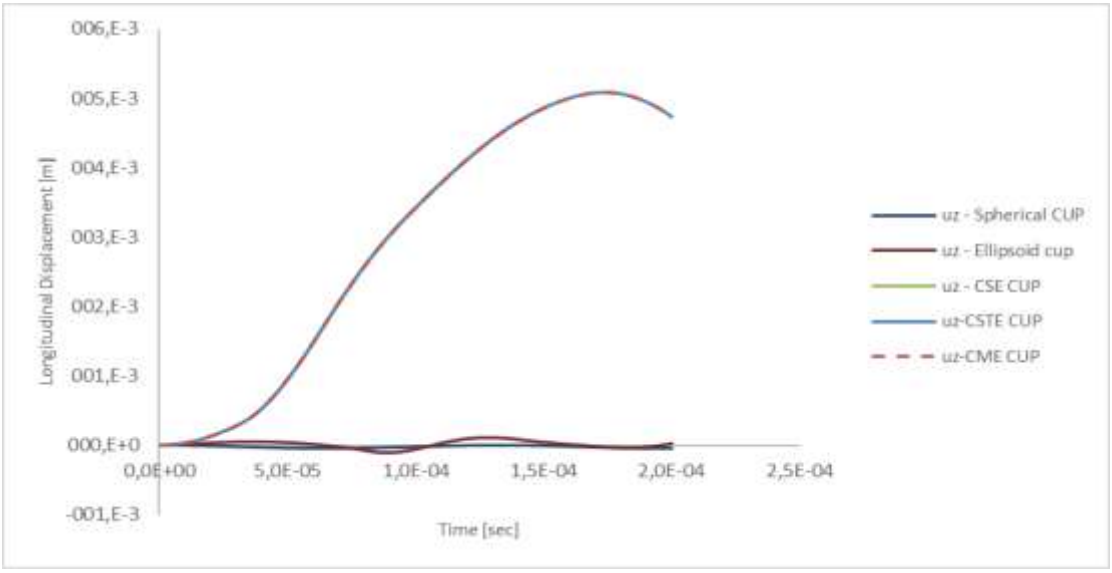
006,E-3
005,E-3
004,E-3
003,E-3
002,E-3
001,E-3
000,E+0
-001,E-3
Longitudinal Displacement [m]
0,0E+00
5,0E-05
1,0E-04
1,5E-04
2,0E-04
2,5E-04
Time [sec]
uz - Spherical CUP
uz - Ellipsoid cup
uz - CSE CUP
uz-CSTE CUP
uz-CME CUP

(*c*)

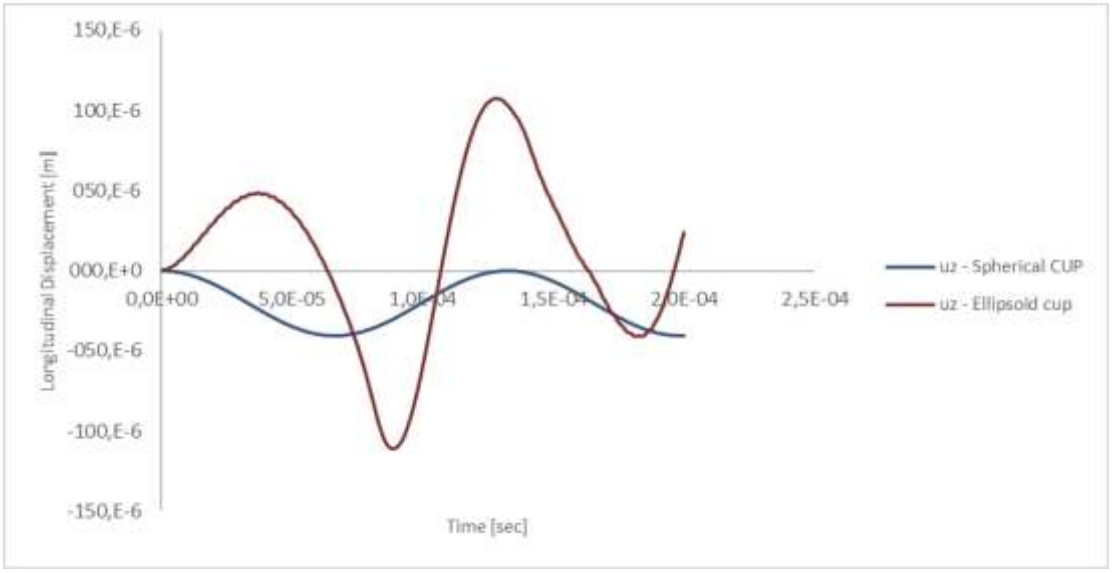
150,E-6
100,E-6
050,E-6
000,E+0
-050,E-6
-100,E-6
-150,E-6
Longitudinal Displacement [m]
0,0E+00
5,0E-05
1,5E-04
2,5E-04
Time [sec]
uz - Spherical CUP
uz - Ellipsoid cup

(*d*)

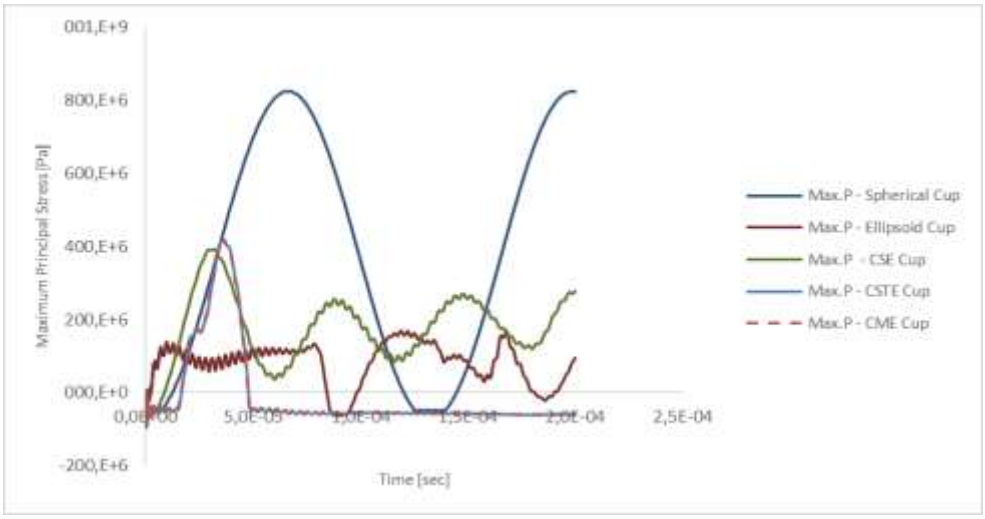

Fig. 5: FE model results for several container cup ending-part shapes: (*a*) u_r - radial displacements for all five shapes (*b*) u_z – all shapes longitudinal displacements (*c*) Zoom–in of (*b*) regarding the results of ellipsoid and spherical shapes (*d*) Maximum principal stress results.

(*a*)

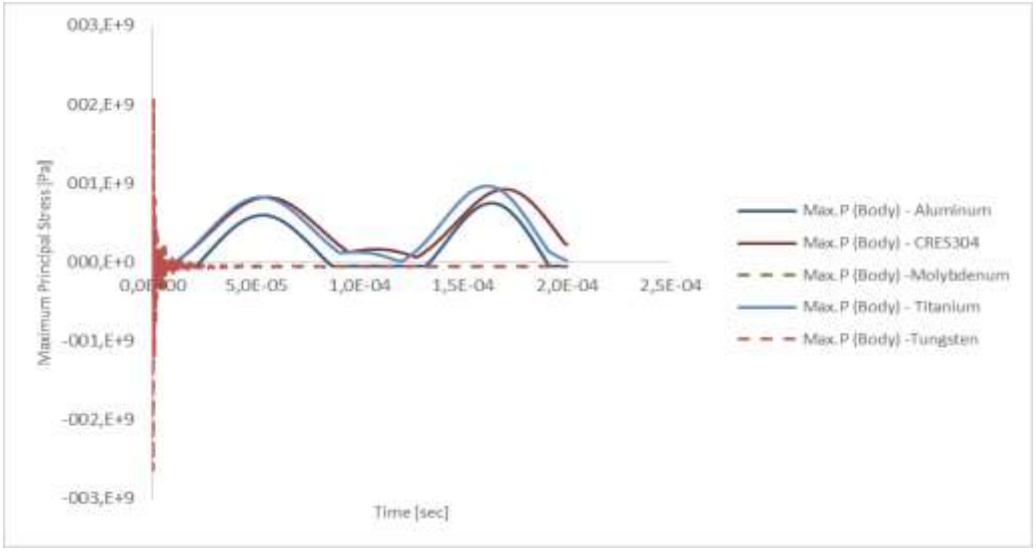

(*b*)

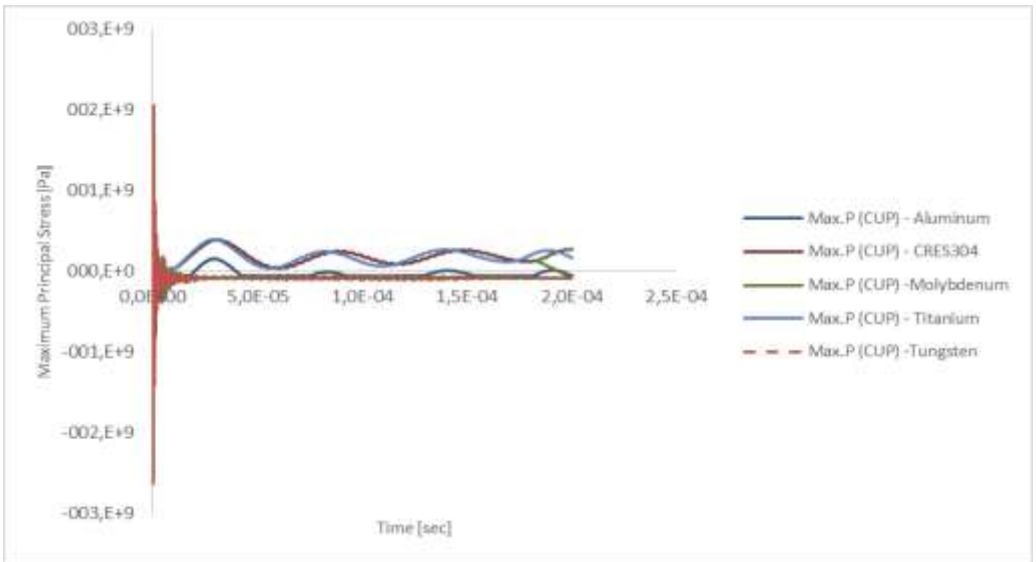

Fig. 6: CSE FE model Maximum principal stress results for a container made of different materials: (*a* Body shape region (*b*) Cup shape region.

Contribution of Individual Authors to the Creation of a Scientific Article (Ghostwriting Policy)

The author contributed in the present research, at all stages from the formulation of the problem to the final findings and solution.

Sources of Funding for Research Presented in a Scientific Article or Scientific Article Itself

No funding was received for conducting this study.

Conflict of Interest

The author (Jacob Nagler) declares that he has no conflicts of interest.